

# Dual Drug Delivery in Cancer Therapy Using Graphene Oxide-Based Nanoplatfoms

Ludmila Žárská, Eoin Moynihan, Arianna Rossi, Giada Bassi, Pavlína Balatková, Elisabetta Campodoni, Maria Galiana Cameo, Monica Montesi, Diego Montagner,\* Vaclav Ranc,\* and Silvia Panseri\*


Many types of cancer are currently treated using a combination of chemotherapeutics, but unfortunately, this strategy is considerably limited by severe side effects. The current development of nanocarriers enables the use of multiple drugs anchored on one unique platform thus enhancing the initiated therapeutic effect and minimizing the possibility of drug resistance. In this context, a graphene-oxide-based 2D nanoplatfom is developed, which is functionalized using highly branched polyethylene-glycol and a multimodal set of two drugs with various mechanisms of action, namely Pt-based complex (a Pt(IV) prodrugs based on cisplatin) and doxorubicin (DOX). We performed in vitro 2D screening on two cancer cell lines, namely glioblastoma and osteosarcoma, that were selected as models of two aggressive tumors that remain a massive challenge in oncology. The therapeutic effect of the developed nano-platfom is higher at lower concentrations (15  $\mu\text{M}$  of Pt-drug, 0.6  $\mu\text{M}$  DOX) compared to the impact of the free drugs. This indicates a possible positive effect of the accumulation and transport of the drugs using this nanoplatfom. Results obtained on 3D cell models using MG63 osteosarcoma cells uncovered an understandable lowered diffusion profile of the developed nanoplatfoms, compared to the application of free drugs.

## 1. Introduction

It has been more than 35 years since the “war on cancer” was declared, and yet, the discovery of efficient and selective anticancer drugs remains a significantly challenging endeavor. Despite considerable progress in genomics and proteomics, the observed increase in approved drugs in the past decade did not match the rising costs associated with cancer research. Nonetheless, cancer chemotherapy has evolved from the use of cytotoxic drugs with potentially life-threatening side effects to less toxic approaches based on hormonal therapy or gene therapy, among others. Still, numerous cancer patients are, in general, treated with platinum-based complexes, often as a part of multi-drug combinations that include, in most cases, two other active ingredients. To enhance effectiveness and mitigate the adverse effects of current anticancer drugs, including platinum-based complexes, researchers in recent decades have conducted extensive

L. Žárská, V. Ranc  
Regional Centre of Advanced Technologies and Materials  
Czech Advanced Technology and Research Institute  
Palacký University Olomouc  
783 71 Olomouc, Czech Republic  
E-mail: vaclav.ranc@upol.cz

E. Moynihan, M. G. Cameo, D. Montagner  
Department of Chemistry  
Maynooth University  
W23 F2H6 Maynooth, Co. Kildare, Ireland  
E-mail: Diego.Montagner@mu.ie

 The ORCID identification number(s) for the author(s) of this article can be found under <https://doi.org/10.1002/anbr.202400026>.

© 2024 The Authors. Advanced NanoBiomed Research published by Wiley-VCH GmbH. This is an open access article under the terms of the Creative Commons Attribution License, which permits use, distribution and reproduction in any medium, provided the original work is properly cited.

DOI: 10.1002/anbr.202400026

A. Rossi, G. Bassi, E. Campodoni, M. Montesi, S. Panseri  
Institute of Science  
Technology and Sustainability or Ceramics – National Research Council of Italy  
48018 Faenza, RA, Italy  
E-mail: silvia.panseri@issmc.cnr.it

A. Rossi  
Department of Chemical, Biological  
Pharmaceutical and Environmental Sciences  
University of Studies of Messina  
98122 Messina, ME, Italy

G. Bassi  
Department of Neuroscience  
Imaging and Clinical Sciences  
University of Studies G. d'Annunzio  
66100 Chieti-Pescara, CH, Italy

P. Balatková, V. Ranc  
Institute of Molecular and Translation Medicine  
Faculty of Medicine and Dentistry  
Palacký University in Olomouc  
Hnevotinska 5, CZ-779 00 Olomouc, Czech Republic

investigations into nanoparticle drug delivery systems (DDSs).<sup>[1]</sup> Among many various materials, graphene has gained significant attention in the field of DDSs, primarily due to its already proven physical and chemical properties.<sup>[2,3]</sup> This nanomaterial comprises a single layer of sp<sup>2</sup>-hybridized carbon atoms, forming a 2D structure with a large specific surface area. This unique characteristic of graphene allows a significant drug load efficacy.<sup>[2,4]</sup> Graphene oxide (GO), which is derived from graphene, contains structural hydroxyl, carbonyl, carboxyl, and epoxide functional groups, which present interesting reactive nuclei contributing to GO's remarkable water solubility, biocompatibility, and multifunctionality. These parameters are crucial for effectively delivering anticancer drugs.<sup>[2,5,6]</sup> To minimize possible cytotoxicity and enhance cellular uptake of GO, recent research has investigated the utilization of biomimetic compounds, including polyethylene glycol (PEG).<sup>[7]</sup> These findings indicate that the presence of PEG further enhances the stability and solubility, reduces aggregation, and extends the enhanced permeability and retention (EPR) effect of the GO.<sup>[8,9]</sup>

Although many single-drug nanocarriers designed for controlled release and targeted delivery in chemotherapy were reported, their adoption in clinical phases still faces significant bottlenecks. Challenges include poor water solubility and limited drug bioavailability.<sup>[10]</sup> Low bioavailability requires the use of higher doses of the drug, which may lead to dose-dependent toxicity.<sup>[11]</sup> Moreover, prolonged treatment with a single drug can eventually lead to drug resistance, which further complicates the therapy.<sup>[12]</sup> Therefore, the development of multidrug nanocarrier-based delivery systems is of high importance.<sup>[10,11,13]</sup>

Combining different drugs offers the advantage of reducing the individual drug doses required without compromising the effectiveness of cancer treatment. Besides the benefits mentioned previously, this approach helps reducing the risk of multidrug resistance (MDR) and cancer recurrence.<sup>[14]</sup>

Here we focused on the synthesis of a potentially interesting dual drug delivery nanoplatfoms involving a Pt(IV) complex pro-drug based on cisplatin scaffold (further labeled as Pt) and doxorubicin (further labeled as DOX). The nanoplatfoms consist of a PEGylated graphene-oxide hierarchy, which previously demonstrated the ability to improve the anticancer efficacy of Pt-based anticancer complexes.<sup>[15]</sup> The structures of the two drugs used in this study and the experimental design are shown in **Figure 1**. Here, the developed nanoplatfoms utilize GO as a framework, which was further decorated using a highly branched PEG structure (8-armed) functionalized with -NH<sub>2</sub> groups. The amine groups are used to covalently bind the Pt drugs via an amide coupling reaction, while DOX was bind electrostatically on the GO framework. We performed physicochemical assessments to characterize key physico-chemical parameters of the nanoplatfoms, including the topography, morphology, electronic properties, and loading capacity to accommodate Pt and DOX drugs. Furthermore, we conducted a standard 2D *in vitro* screening on two cancer cell lines, glioblastoma and osteosarcoma, which were selected as models of two aggressive tumors that remain challenging in oncology. Based on the most promising results obtained on 2D models, we performed a more complex and predictive 3D *in vitro* model test by using a biomimetic scaffold that better recapitulates the complexity of the tumor.

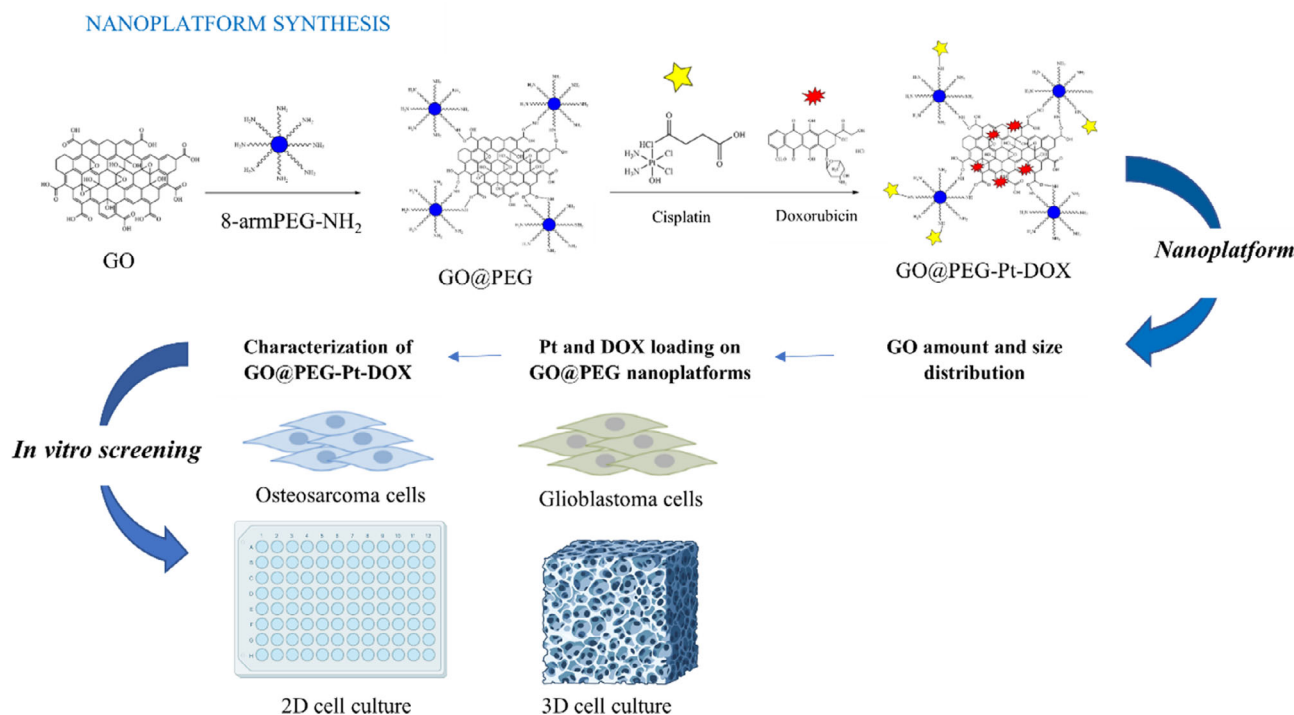


**Figure 1.** Schematic representation of the synthesis of GO@PEG nanoplatfoms and their functionalization using Pt and doxorubicin followed by their study on 2D and 3D *in vitro* models.

## 2. Results and Discussion

### 2.1. Characterization of GO-Based Nanoplatfoms

The combination of approaches previously described by Ma and Chen<sup>[16,17]</sup> (for details, see Materials and Methods, Section 3.2) led to a targeted reduction in the average size of graphene oxide (GO) that was originally present in the respective stock solution. The initial lateral average size of GO flakes was 17  $\mu\text{m}$ . Applying the described procedure reduced an average lateral particle size below 210 nm for 74% of the statistical population of GO flakes ( $n = 2077$ , **Figure 2C**). Analogically, the average height decreased from 130 nm (stock dispersion) to 1.1 nm. All values were obtained from the measurements using atomic force microscopy (AFM) as shown in **Figure 2A** and S1, Supporting Information, respectively. More information can be found in the complete histogram illustrating the distribution of present flake sizes, which is available in **Figure S2**, Supporting Information.

Next, pristine GO flakes were subjected to functionalization using a highly branched 8-arm PEG-NH<sub>2</sub>. This modification significantly changed the height profile from 1.1 nm (equivalent to two carbon layers, as shown in **Figure S1**, Supporting Information) to 45 nm (**Figure 2B**). This indicates a successful immobilization of PEG structures on the surface GO. The progress of the functionalization using PEG was further studied using electron microscopy (TEM and SEM), with results shown in **Figure 2D–F**. **Figure 2D** shows an SEM micrograph of the pristine GO, where the structure of thin flakes can be observed.

TEM micrographs (**Figure 2E,F**) show morphological changes induced by the functionalization using PEG, which are visible as amorphous structures localized on the GO flake in **Figure 2F**.

Consecutive functionalization of the PEG@GO nanoplatfoms using selected drugs, namely Pt and DOX (as described in Section 2.4. of Materials and Methods), was evaluated by Raman, fourier transform infrared spectroscopy (FTIR) spectroscopy and parallel measurements of zeta potential. The zeta potential changes that occurred due to GO size modification, GO PEGylation, and drug binding are shown in **Figure 3A**, where the errors of the measurements are reflected by the size of the respective data points. First, the initial zeta potential of the stock dispersion was moderately negative ( $-34.4$  mV). This value is given by the high numbers of negatively charged functional groups. The reduction in the flake sizes led to the increase of the potential to a less negative value ( $-2.7$  mV) due to the repositioning of the charge over the larger obtained surface. Functionalization of GO using PEG led to a further increase of the potential to 3.7 mV due to the presence of structural amino groups. Loading of Pt-based drugs led to partial saturation of the amino groups and decreased the zeta potential backward to negative values ( $-2.8$  mV). Finally, loading the DOX (presence of the free amino group) led to a slight increase of the zeta potential back to 2.7 mV. **Figure 3A** also shows the value for GO@PEG-DOX platform to illustrate the sole effects of the DOX on the resulting zeta potential. The loading of the Pt and DOX was next evaluated using FTIR and Raman. **Figure 3B** shows IR spectra for the starting material, namely

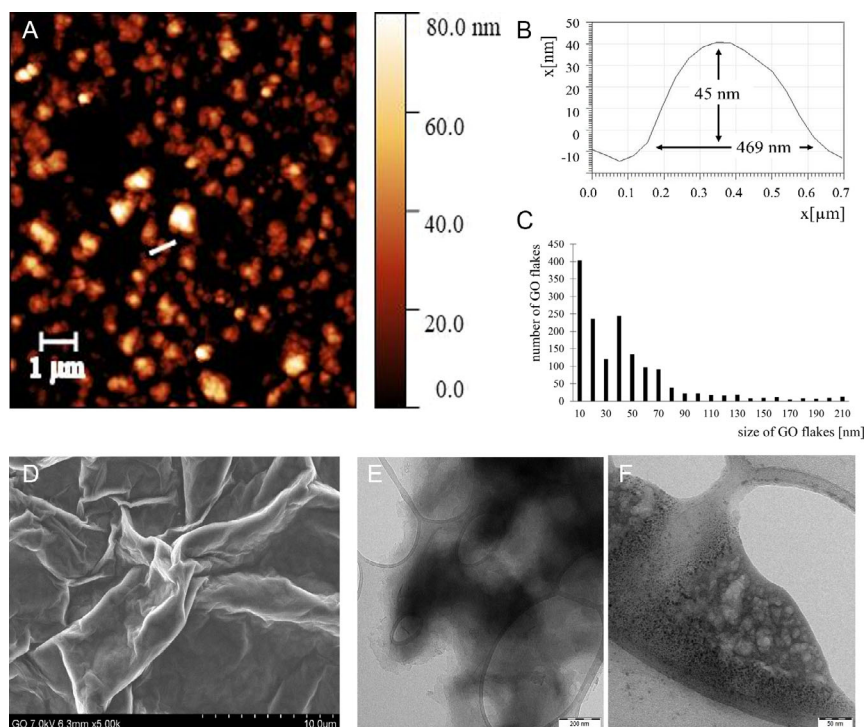


**Figure 2.** A) PEGylated GO flakes were displayed by AFM, and B) for marked GO flakes, the height profile was specified. C) The GO flakes in the supernatant determined the characteristic size distribution. D) Graphene oxide in stock solution was displayed by scanning electron microscopy (SEM) in image. E) Transmission electron microscopy (TEM) was used to determine morphological changes in GO-based nanoplatfom and F) PEGylated GO.

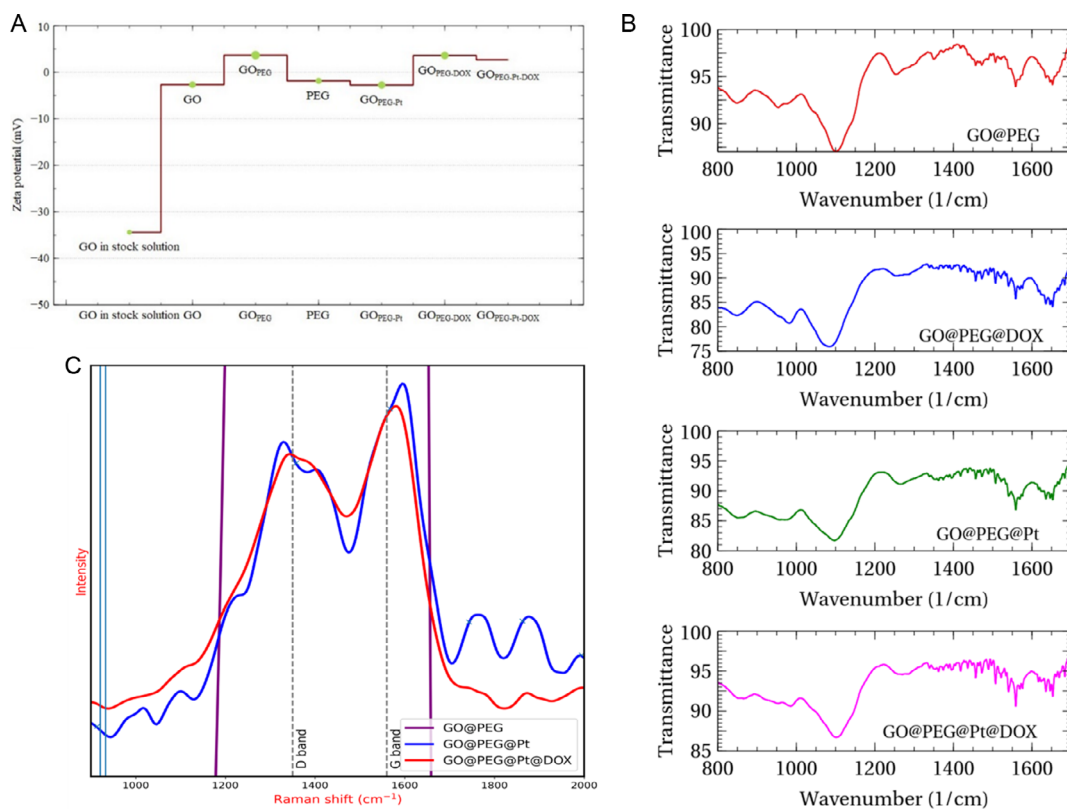


**Figure 3.** A) Changes in zeta potential were determined for GO in stock solution and GO in the supernatant, and subsequently for free PEG, PEGylated GO, and the nanoplatform with drugs. B) The presence of Pt and DOX on GO@PEG was demonstrated by characteristic IR spectra obtained at four steps of the synthesis. C) The successful binding of Pt and DOX drugs to PEGylated GO was also demonstrated by Raman spectra.

GO@PEG, which contain spectral bands characteristic for PEG, including vibrations of C–H ( $1455\text{ cm}^{-1}$ ) and C–O ( $1100\text{ cm}^{-1}$ ) groups. Functionalizing the platform with Pt considerably altered the Amide III spectral band present at  $1100\text{ cm}^{-1}$ . The loading of DOX is accompanied by the formation of the spectral band at  $1060\text{ cm}^{-1}$ , which again partially overlaps with the Amide III band. Raman spectra of the functionalized platform GO@PEG-Pt-dox (Figure 3C) show a considerable blue shift in the position of the G band from  $1590$  to  $1620\text{ cm}^{-1}$  and the formation of an additional spectral band at  $1400\text{ cm}^{-1}$ . Moreover, to investigate the presence of doxorubicin on the surface of the functionalized GO@Pt-dox nanoplatform, we performed also experiments using UV/Vis spectroscopy. Results are summarized in Figure S3, Supporting Information, where it can be seen that binding of the doxorubicin on the surface of the GO@PT platform leads to the formation of characteristic spectral profile in the respective data. The loading efficiency (LE) of the GO@PEG nanoplatform was found to be 56% for Pt and 38% for DOX. The nature of the anchoring of Pt and DOX suggests that doxorubicin will be released in the first phase of the interaction of drug nanoplatform with cellular environment due to the lower pH values in cancerous cells. Platinum-based complex is covalently attached which suggests an afterward release of this drug by intracellular reduction from Pt(IV) to Pt(II). The stability of the developed nanoplatforms were evaluated for a period of 30 days. Atomic absorption

spectroscopy was utilized to monitor the changes in the content of Pt-based drugs. Based on the results, it can be stated that the material is stable for at least 30 days without any significant loss of bound drugs from the surface of the nanostructures. The stability of the developed nanoplatforms was evaluated for 30 days. Atomic absorption spectroscopy was utilized to monitor the changes in the content of Pt-based drugs. Based on the results, it can be stated that the material is stable for at least 30 days without any significant loss of bound drugs from the surface of the nanostructures.

## 2.2. Biological Effect of the 2D Nanoplatform on 2D Cellular Models

Osteosarcoma and glioblastoma are two of the most aggressive tumors, which still represent a challenge in medicine and the scientific community. Specifically, osteosarcoma is the most common malignant bone tumor in children and young adults,<sup>[18]</sup> and the current treatments include chemotherapy with cisplatin and doxorubicin, as well as surgical interventions.<sup>[19,20]</sup> Glioblastoma is the most common high-grade primary malignant brain tumor, characterized by an inferior prognosis. The most common treatments currently used for glioblastoma include surgery, radiotherapy, and chemotherapy.<sup>[21]</sup> In both cases, new medical advancements are needed to overcome the current limitations and reduce the side effects of chemotherapy.

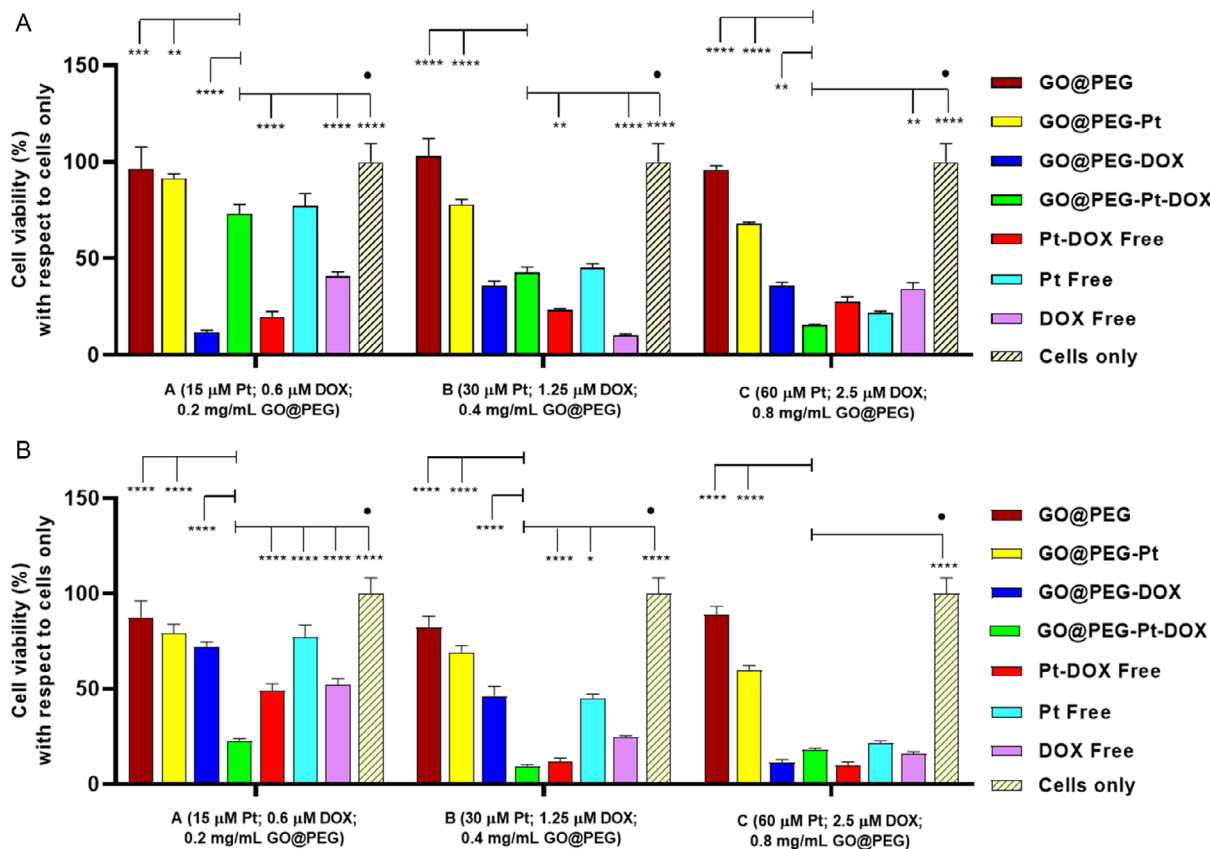
MG63 (osteosarcoma cell line) and U-87 (glioblastoma cell line) were selected to test the efficacy of the developed nanoplatforms.

A preliminary standard 2D in vitro screening was conducted on both cell lines. Briefly, the cell viability was assessed by MTT assay after 72 h of incubation in the presence of the nanoplatforms and their respective controls based on three different Pt concentrations (Table 1). The results showed that overall, all the drug-loaded compounds and their relative drug-free

controls induced a significant reduction of cell viability in both cell lines at all concentrations tested, compared to cells only ( $p$ -value  $\leq 0.0001$ ) (Figure 4). Specifically, looking at the graphs, the GO@PEG-Pt-DOX showed a different behavior in the two cell lines, reporting a more cytotoxic activity on MG63 cells, compared to U-87 cell line. In detail, in the MG63 cells, a significant reduction of cell viability was reported by GO@PEG-Pt-DOX compared to GO@PEG-DOX and

**Table 1.** Concentrations of each compound in the tested samples.

Sample/Concentration level	A			B			C		
	Pt [ $\mu\text{M}$ ]	DOX [ $\mu\text{M}$ ]	GO@PEG [ $\text{mg mL}^{-1}$ ]	Pt [ $\mu\text{M}$ ]	DOX [ $\mu\text{M}$ ]	GO@PEG [ $\text{mg mL}^{-1}$ ]	Pt [ $\mu\text{M}$ ]	DOX [ $\mu\text{M}$ ]	GO@PEG [ $\text{mg mL}^{-1}$ ]
GO@PEG-Pt-DOX	15	0.60	0.20	30	1.25	0.40	60	2.50	0.80
GO@PEG-Pt	15	–	0.20	30	–	0.40	60	–	0.80
GO@PEG-DOX	–	0.60	0.20	–	1.25	0.40	–	2.50	0.80
GO@PEG	–	–	0.20	–	–	0.40	–	–	0.80
Pt-DOX	15	0.60	–	30	1.25	–	60	2.50	–
Pt	15	–	–	30	–	–	60	–	–
DOX	–	0.60	–	–	1.25	–	–	2.50	–



GO@PEG-Pt ( $p$ -value  $\leq 0.0001$ ), but most importantly compared to Pt, DOX and a combination of Pt-based complexes and DOX at both 15 and 30  $\mu\text{M}$  ( $p$ -value  $\leq 0.0001$  and  $\leq 0.05$ ), suggesting a higher cytotoxic activity by double-loaded nanoplatform starting from the lowest concentration tested compared to single-loaded ones and also to free drugs, as sign of a higher cell internalization of both drugs only loaded to GO@PEG. However, only a significant cytotoxicity compared to GO@PEG-Pt was preserved by GO@PEG-Pt-DOX at the highest concentration tested (Figure 4A). In the MG63 cells, the biological activity of GO@PEG-Pt-DOX seemed to be more gradual and dose-dependent, showing a significant reduction of cell viability only concerning GO@PEG-Pt at 15 and 30  $\mu\text{M}$  ( $p$ -value  $\leq 0.01$  and  $\leq 0.0001$ ). However, it is the GO@PEG-DOX showing the highest reduction in cell viability at 15  $\mu\text{M}$ , with a significant difference compared to GO@PEG-Pt-DOX ( $p$ -value  $\leq 0.0001$ ). Moreover, significant cytotoxicity was preserved by free drugs,

especially DOX and Pt-DOX, at 15 and 30  $\mu\text{M}$ , compared to GO@PEG-Pt-DOX ( $p$ -value  $\leq 0.0001$  and  $\leq 0.01$ ), suggesting a higher biological activity in the absence of the nanoplatforms. Surprisingly, this trend was completely inverted at 60  $\mu\text{M}$ , where a significant reduction of cell viability was shown by GO@PEG-Pt-DOX, not only concerning GO@PEG-Pt ( $p$ -value  $\leq 0.0001$ ) and GO@PEG-DOX ( $p$ -value  $\leq 0.01$ ), but also concerning DOX ( $p$ -value  $\leq 0.01$ ) (Figure 4B). Finally, it is possible to assert that the double-loaded nanoplatform showed a cell line-dependent behavior, with higher cytotoxicity at the lowest concentration and dose-dependent cytotoxicity in MG63 and U87 cells, respectively. Most importantly, no signs of cytotoxicity were reported by the GO@PEG alone in both cell lines and at all concentrations tested, suggesting that the potential cell mortality could be solely attributable to the potential increase of the drug delivery inside the tumor cells by the innovative nanoplatforms (Figure 4).

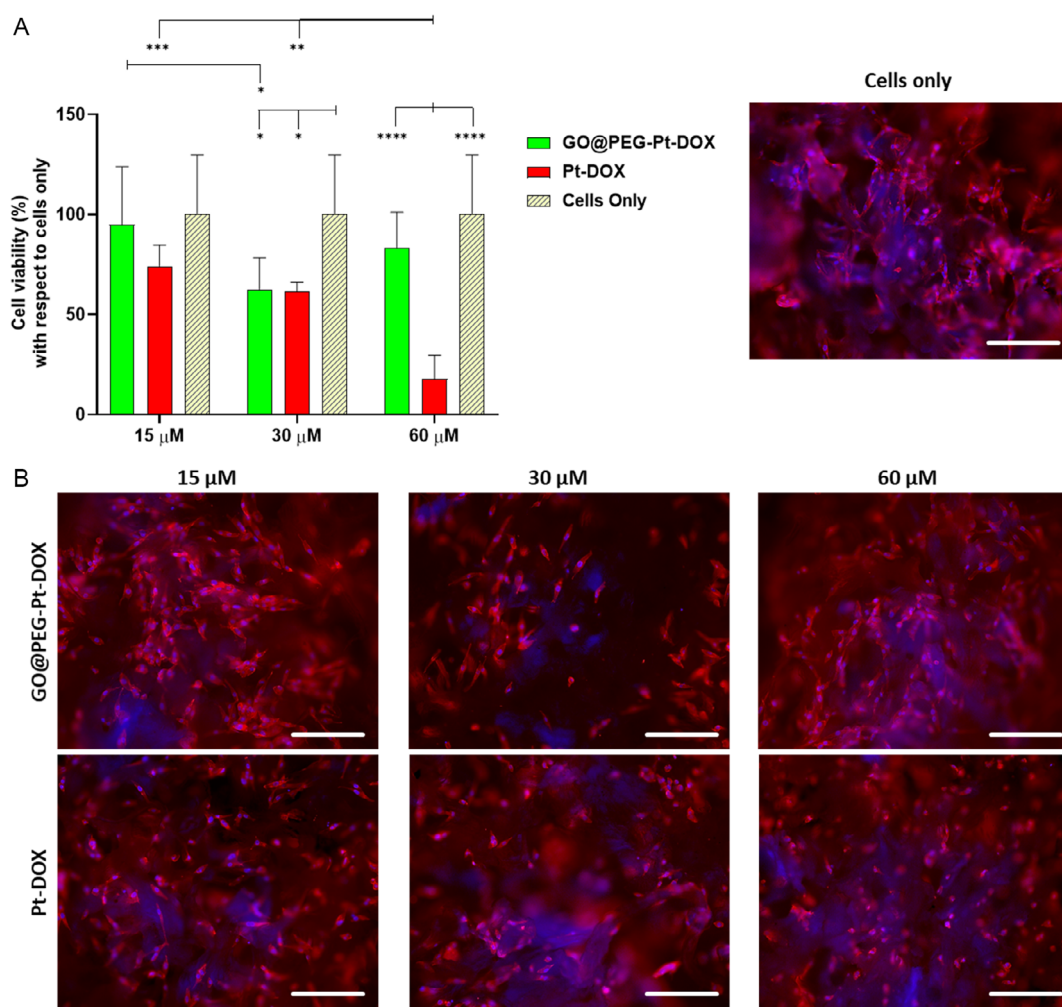


**Figure 5.** 3D OS models: MTT assay and cell morphology. GO@PEG-Pt-DOX and Pt-DOX were tested on 3D OS models at the 15, 30, and 60  $\mu\text{M}$  concentrations, using cells only as a negative control. After 72 h incubation, a cell viability assay A) and a cell morphology evaluation B) were performed. Data from the MTT assay are shown in the graph as a percentage (%) mean compared to cells only  $\pm$ SD. Statistically significant differences are reported in the graph: \* $p$ -value  $\leq 0.05$ , \*\* $p$ -value  $\leq 0.01$ , \*\*\* $p$ -value  $\leq 0.001$  and \*\*\*\* $p$ -value  $\leq 0.0001$ . Fluorescence analyses stained cell nuclei in blue (DAPI) and F-actin filaments in red. Scale bars: 200  $\mu\text{m}$ .

### 2.3. Biological Effect of the 2D Nanoplatfoms on 3D Cellular Models

Considering the promising results of low-dose cytotoxicity on the MG63 cell line, we decided to further characterize the GO@PEG-Pt-DOX using a 3D osteosarcoma (OS) model as a more predictive in vitro platform resembling the in vivo tumor microenvironment (Figure 5). It is well-known that conventional in vitro 2D cell cultures do not faithfully represent the complexity of the tumor in vivo, providing unreliable results.<sup>[22,23]</sup> To create an advanced 3D in vitro OS model, MG63 cells were seeded on the bone-mimetic scaffold MgHA/Coll, a well-established material for regenerative medicine purposes, which is obtained through the reproduction in the lab of the biomineralization process that typically occurs during bone formation and growth.<sup>[24]</sup> Moreover, the 3D OS models were grown for three days before the addition of the compounds, with the final aim of obtaining a fully colonized tissue-like model. GO@PEG-Pt-DOX was added to the 3D OS models at the same concentrations tested on the 2D screening, and Pt-DOX was added as the control group. The cell viability assay after 72 h of incubation showed that both GO@PEG-Pt-DOX and Pt-DOX are less effective in the 3D OS model compared to the results obtained on 2D cell culture, confirming the importance of using relevant and more complex cell culture systems to test innovative anti-cancer platforms (Figure 5A). In general, less than 50% of cells died in the presence of both compounds, even at the highest concentration, with a slight significant reduction of cell viability only at 30  $\mu\text{M}$ , compared to cells only ( $p$ -value  $\leq 0.05$ ). The only exception is Pt-DOX, where dose-dependent cytotoxicity is observed, albeit to less extent compared to 2D cell cultures and with significant differences only at the highest concentration tested compared to both cells only and GO@PEG-Pt-DOX ( $p$ -value  $\leq 0.0001$ ). This reduced effectiveness of the nanoplatfoms, compared to the Pt-DOX, could be attributed to the challenges faced by the drug-loaded systems in reaching the cells. Indeed, in this 3D cell culture, a highly intricate network of cells is fused nearly, with the collagen-based matrix of the scaffold. Likely, the cells that penetrated deeper into the scaffold were not reached by an adequate concentration of any of the two tested drugs (Figure 5A). To confirm these data, an Actin/Dapi staining was performed to assess the cytoskeleton and nuclei shape, and to evaluate the cellular state. As shown in Figure 5B, the cells treated with the lowest concentration exhibited a cell density and a morphology comparable to the cells only, suggesting the absence of any cytotoxic effect by compounds. However, at higher concentrations, the cytoskeleton appeared slightly compromised, and the cell number was drastically reduced only in Pt-DOX, confirming the overall results of the MTT assay.

Furthermore, to confirm the critical role of the 3D OS model, we conducted a colonization-level evaluation to determine whether the nanoplatfoms efficiently affect the cell migration inside the material. For this purpose, as shown in Figure 6, the cell migration analysis was conducted and presented as normalization concerning the 3D OS models at 0 h (before compound addition). Specifically, six random measurements of the migration distance ( $\mu\text{m}$ ) by the cells from the seeding surface to the inner part of the 3D OS model were performed for both

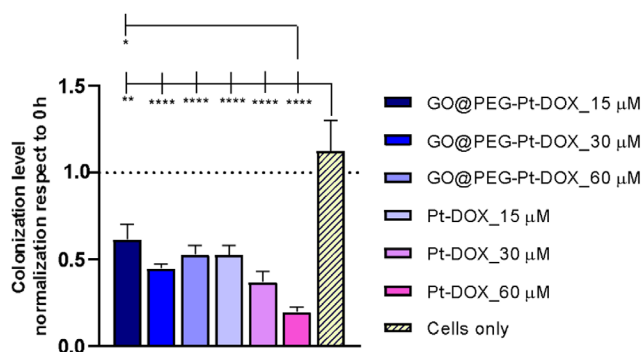


**Figure 6.** Cell migration in 3D OS model. The colonization level of the 3D OS models treated with compounds and cells only normalized with respect to colonization at 0 h. Data are shown as normalization with respect to the 3D OS model at 0 h  $\pm$  SEM. Statistically significant differences are reported in the graph: \* $p$ -value  $\leq 0.05$ , \*\* $p$ -value  $\leq 0.01$ , and \*\*\*\* $p$ -value  $\leq 0.0001$ .

GO@PEG-Pt-DOX, Pt-DOX, and cells only. This was compared to the 3D OS model at 0 h to assess the potential inhibitory effect on cell migration ability caused by the compounds. The results showed that the treated 3D OS models displayed a significant reduction of cell migration ( $p$ -value  $\leq 0.0001$  and  $p$ -value  $\leq 0.01$ ) compared to the cells-only group. In contrast to the MTT assay, these findings may indicate that the nanoplatfoms have the potential to inhibit the invasiveness of cells in colonizing the material, without causing cell death. This suggests the possibility of using this nanoplatfom to prevent further metastatic spread of the disease. Metastasis occurs when cancer cells escape from the primary tumor site and travel to invade new tissues or organs. The invasion capability of cancer cells involves the production of pseudopodia, the formation of new adhesions, the release of old adhesions, tissue penetration, and migration to new sites.<sup>[25]</sup> However, no statistically significant differences were observed among the compounds at any tested concentration, except for Pt-DOX at 60  $\mu\text{M}$  ( $p$ -value  $\leq 0.05$ ). This confirms the dose-dependent activity of these drugs on the 3D OS models, consistent with the results obtained from the MTT assay.

In conclusion, these results emphasize the significance of using more predictive 3D in vitro models for screening purposes. While promising cytotoxicity results were observed with GO@PEG-Pt-DOX, particularly on MG63 cells, in standard 2D cell cultures, the 3D OS model study revealed that the double-loaded nanoplatfoms did not significantly reduce cell viability compared to the free drugs. However, the cell migration analysis suggested that the activity of GO@PEG-Pt-DOX might be associated with its ability to impede cell mobility during scaffold colonization.

The inhibition of migration observed on a 3D model by drugs underscores the importance of utilizing more advanced experimental platforms for comprehensive assessment. This study represents an initial exploration, and additional research is necessary to optimize some parameters (e.g., timing; dose) due to the considerable differences between 3D and 2D models, together with specific biological analysis to better clarify the molecular mechanisms.

Overall, the role of the 3D OS model in drug/nanoplatfom uptake is confirmed, and this discovery holds promise for future platform optimization, aiming to achieve a meaningful impact, especially in a 3D setting. This, in turn, enhances the prospects of in vivo efficacy.

### 3. Conclusion

Dual drug delivery systems represent a groundbreaking approach in cancer therapy by simultaneously or sequentially delivering of two chemotherapeutics with different modes of action. Their significance lies in the synergistic effect these drugs create, targeting multiple aspects of cancer cells or their environment. This study demonstrated the versatility of GO-based nanoplatfoms in the development of drug-delivery systems for a controlled loading and transport of two anticancer drugs, such as a cisplatin derivate and doxorubicin on a single platform consisting of graphene oxide functionalized using eight-branch polyethylene glycol. The achieved loading efficiency of the GO@PEG nanoplatfom is 56% for Pt and 38% for DOX, where samples were normalized to a concentration of platinum and diluted at 15, 30, and 60  $\mu\text{M}$  concentrations of Pt. These samples, together with negative controls (GO, GO@PEG) and pure compounds were studied from the point of their action on cancer cells. Glioblastoma cell line U87 and osteosarcoma cell line MG63 were selected for the initial tests due to their considerably different behavior and thus their various abilities to cope with drugs. We showed that the developed platfoms can transport both loaded drugs and that the therapeutic effect is higher at lower concentrations (15  $\mu\text{M}$  Pt), compared to the effect of free drugs. This result is comparable to the free drugs when concentrations of drugs are increased, indicating a possible positive effect of the transport of drugs using the nanoplatfom. Next, we performed studies using an advanced 3D scaffold-based model seeded with MG63 osteosarcoma cells. The obtained results uncovered an understandable lowered diffusion profile of the developed nanoplatfoms, compared to the application of free drugs. The results further obtained on cell migration showed that the treated 3D OS models displayed a significant reduction of cell migration compared to the cells-only group. In contrast to the MTT assay, these findings indicate that the nanoplatfoms have the potential to inhibit the invasiveness of cancer cells in colonizing the material, without further causing a cell death. By combining drugs with different mechanisms of action, these systems could enhance therapeutic efficacy while potentially overcoming drug resistance and they offer a personalized treatment approach and aim to minimize side effects by precisely targeting tumor sites.

### 4. Experimental Section

**Pt-Based Drug:** The cisplatin-based drug (Pt) is a Pt(IV) complex based on cisplatin scaffold containing a carboxylic acid in axial position. The compound has been prepared as previously reported.<sup>[15]</sup> Briefly, cisplatin was oxidized to oxoplatin (cis,cis,trans-[Pt(NH<sub>3</sub>)<sub>2</sub>Cl<sub>2</sub>(OH)<sub>2</sub>] with H<sub>2</sub>O<sub>2</sub> and then reacted with succinic anhydride to produce the Pt(IV) prodrug (Pt) tethering a carboxylic acid in axial position that is used to covalently bind the compound to the GO nanoplatfoms functionalized with 8-armed PEG-NH<sub>2</sub>. Cisplatin will be then released in the active form by intracellular reduction of the Pt(IV) (Pt) pro-drug.<sup>[26]</sup>

**GO Flake Size Optimization:** The initial material for the study was commercially procured GO obtained from Sigma Aldrich, Saint Louis, MO, USA. The flake sizes were adjusted and selected using a combined approach based on two previously documented procedures.<sup>[16,17]</sup> In summary, the GO stock solution at a concentration of 4 mg mL<sup>-1</sup> was diluted to 400  $\mu\text{g mL}^{-1}$  in the PBS buffer. This diluted solution of GO underwent ultrasonic sonication in a Sonorex Digitec DT 103 H ultrasonic bath (Bandelin, Berlin, Germany) at 70 °C for 6 h. The sample was subsequently subjected to agitation for 18 h using a Heidolph Unimax 1010 shaker (500 RPM, 65 °C) from Heidolph, Schwabach, Germany, and was sonicated again for 6 h in the ultrasonic bath at 70 °C. Larger flakes were eliminated through centrifugation (Benchtop 4–16 K, 21 191 RCF, 5 min), and the resultant GO dispersion-containing supernatant was utilized for all successive experiments.

**PEGylation of GO:** A quantity of 25 mg of 8-arm polyethylene glycol-amine (labeled as PEG-NH<sub>2</sub>, 10 kDa) obtained from Sigma-Aldrich, St. Louis, MI, USA, was added into the 5 mL of previously prepared GO dispersion. The mixture underwent a 10-minute sonication process. Following this, 40  $\mu\text{L}$  of N-(3-Dimethylaminopropyl)-N'-ethylcarbodiimide hydrochloride (EDC, Sigma-Aldrich) at a concentration of 5 mg mL<sup>-1</sup> was gradually added to the mixture. After 24 h of stirring (500 RPM, 65 °C), a second round of stirring and sonication followed for 18 h (500 RPM, 65 °C) and 6 h (70 °C) respectively. Infrared spectra of PEGylated GO were acquired using a Nicolet iS5 FTIR spectrometer (Fisher Scientific, Waltham, MA, USA) operating in ATR mode using a ZnSe crystal.

**Pt and DOX Loading on GO@PEG Nanoplatfoms:** The loading process of compound Pt and DOX onto GO@PEG occurred in two steps. Initially, a solution was prepared by combining 25  $\mu\text{L}$  (20 mg mL<sup>-1</sup> stock solution) of Pt and 50  $\mu\text{L}$  (2 mg mL<sup>-1</sup> stock solution) of DOX with 4  $\mu\text{L}$  (50 mg mL<sup>-1</sup> stock solution) of EDC. This mixture was sonicated for 10 min to achieve a uniform, transparent solution, which was then stirred at room temperature for 1 h at a speed of 500 RPM. Subsequently, this Pt, DOX, and EDC solution was introduced into the final 1 mL of GO@PEG, followed by agitation for 24 h at 500 RPM and 23 °C. Any unbound compounds Pt and DOX were eliminated through centrifugation at 21 191 RCF for 10 min. The quantity of anchored Pt was determined using atomic absorption spectroscopy (AAS) and electrostatically attached DOX by UV-Vis, with a triplicate measurement (N=3) for both components. The final GO@PEG-Pt pellet obtained was gently resuspended in 1 mL of PBS and then stored at room temperature until use.

**Characterization of GO-Based Nanoplatfoms: Determination of GO Amount and Size Distribution:** The Raman spectra of the GO@PEG nanoplatfoms were acquired employing a Witec Alpha 300 R + Raman spectroscopic system (Witec, Ulm, Germany) with an excitation wavelength of 532 nm. The laser's power on the sample was maintained at 5 mW. To generate each spectrum, 30 micro scans were averaged. For the data presented in Section 3, six spectra were obtained from six different random positions on the flake and were subsequently averaged. The AFM technique was employed to determine the concentration and size distribution of the prepared dispersion. The measured concentration was  $1.5 \times 10^9$  GO flakes/mL, with a median size of 266 nm. An atomic force microscope (AFM, Ntegra spectra, NT-MDT, Moscow, Russia) was utilized for the analysis of GO flake height and size in both the stock solution and the supernatant solution, as well as GO@PEG (Figure S1, Supporting Information). Notably, prior AFM investigations have empirically confirmed the thickness of single-layer graphene to be approximately 1.1 nm,<sup>[27–29]</sup> and this insight was applied here. The AFM technique was also utilized to calculate the amount of GO flakes in 1 mL of the supernatant solution and to analyze the distribution of GO sizes within the supernatant solution.

For AFM imaging, a volume of 5  $\mu\text{L}$  of the sample was deposited onto a mica substrate measuring 0.5 cm in radius. AFM images covering an area of 50  $\times$  50  $\mu\text{m}$  were captured in semi-contact mode using an ACTA-SS-10 tip and a scanning speed of 0.3 Hz. Subsequently, the collected images were processed using the Gwydion software, and the number of GO flakes within each image was analyzed using ImageJ software. This analysis allowed for the determination of the total amount of GO in the



supernatant solution and provided data for size distribution calculations ( $N = 2077$ ).

For scanning electron microscopy (SEM) imaging, a Hitachi SU6600 scanning electron microscope (Hitachi, Tokyo, Japan) was employed. A small droplet of material dispersed in water was deposited onto a carbon tape and air-dried at room temperature to analyze GO in the stock solution. An accelerating voltage of 7 kV was applied for imaging. Similarly, a small droplet of GO@PEG dispersion in water was placed on a copper grid with a carbon film. After air-drying at room temperature, the sample was imaged using an accelerating voltage of 5 kV.

**Characterization of GO-Based Nanoplatfoms: Pt and DOX Loading on GO@PEG Nanoplatfoms:** The loading efficiency of Pt and DOX onto GO@PEG was assessed by analyzing the supernatant obtained through centrifugation during the final step of GO@PEG-Pt-DOX preparation (Section 2.4) using atomic absorption spectroscopy (AAS). The loading ratio of Pt was determined using AAS and UV-Vis for DOX, respectively, and calculated following a previously established definition of loading efficiency.<sup>[29]</sup> Loading efficiency percentage (LE%) is defined as (the concentration of the drug loaded onto GO divided by the initial concentration of the drug) multiplied by 100:

$$LE = \frac{\text{concentration of Pt } \vee \text{ DOX loaded}}{\text{concentration of Pt } \vee \text{ DOX initially}} \times 100\% \quad (1)$$

**In Vitro Biological Study: Cell Culture:** U-87 (ATCC HTB-14) and MG63 (ATCC CRL1427), respectively glioblastoma and osteosarcoma tumour cell lines were purchased from ATCC and used for the in vitro biological evaluation. U-87 cells were cultured in MEM Alpha (Gibco) with 10% fetal bovine serum (FBS) (Gibco) and 1% penicillin/streptomycin mixture (pen/strep) ( $100 \text{ U mL}^{-1}$ – $100 \mu\text{g mL}^{-1}$ ) (Gibco). MG63 cells were cultured in DMEM-F12/Glutamax (Gibco) with 10% FBS and 1% pen/strep. All the cell handling procedures were performed in sterile conditions under a laminar flow hood, and the cells were grown in a controlled atmosphere at 37 °C, 5% CO<sub>2</sub>, and humidity conditions. Cells were detached from culture flasks by trypsinization, centrifuged, and resuspended in an appropriate volume of cell culture media to perform a Trypan Blue Dye Exclusion test to assess cell viability and to count the cells.

**In Vitro Biological Study: Scaffold Synthesis:** To synthesize bone-mimetic scaffolds, a biomimetalization process was designed at ISSMC of CNR of Italy.<sup>[24]</sup> Briefly, an acid aqueous suspension was prepared by dispersing 150 g of type I collagen gel from equine tendon (acidic gel  $10 \text{ mg mL}^{-1}$ , provided by Typeone Biomaterials S.r.l.) was diluted into a phosphoric acid solution (2.4 g in 500 mL; H<sub>3</sub>PO<sub>4</sub>, 85 wt%) (Sigma Aldrich) at room temperature (RT) to obtain an acidic aqueous suspension. Separately, a basic aqueous suspension was obtained by mixing 0.35 g of magnesium chloride (MgCl<sub>2</sub>·6H<sub>2</sub>O, 99 wt%) (Sigma Aldrich) and 2.7 g of calcium hydroxide (Ca(OH)<sub>2</sub>, 95 wt%) (Sigma Aldrich) and in 500 mL of milli-Q H<sub>2</sub>O at RT to obtain a basic aqueous suspension. The acidic suspension was poured into the basic one at 25 °C under continuous stirring and matured for two hours. This led to the nucleation and controlled growth of MgHA nanocrystals onto the collagen fibers, forming the MgHA/Coll hybrid hydrogel which was rinsed three times in milli-Q H<sub>2</sub>O. Finally, to create a 3D porous architecture featured by interconnected porosity, hybrid hydrogel was freeze-dried with specific temperature ramps (−40 and +25 °C) for 48 h under 0.086 mbar vacuum conditions (LIO 3000 PLT, 5PASCAL). The scaffolds were stabilized by dehydrothermal treatment (DHT) crosslinking at 160 °C for 48 h under vacuum (0.01 mbar) essential to preserve the biological cue of the collagen. The scaffolds (ø:6 mm; h:4 mm) named MgHA/Coll\_DHT were sterilized by 25 kGy γ-ray irradiation and used to create the in vitro 3D Osteosarcoma models (3D OS models).

**In Vitro Screening of Compounds in 2D Cell Cultures:** For the 2D screening, MG63 and U-87 cells were seeded at a density of  $8.0 \times 10^3$  cells/well in a 96 well-plate; the day after, the cell culture media was replaced with the compound-conditioned media.

The compounds, here reported as GO@PEG-Pt-DOX and GO@PEG-Pt, were tested at three different concentrations of Pt (15, 30, and 60 μM) as indicated in Table 1; the concentration of DOX and platform GO@PEG

derived from testing the above-reported compounds is reported in the same table for each Pt concentration, and it was used to test GO@PEG-DOX and GO@PEG, respectively. Pt, DOX, and Pt-DOX were used as control groups.

**In Vitro Testing on 3D OS Models:** For developing the in vitro 3D OS models, the scaffolds MgHA/Coll were used as a bone-like matrix in combination with MG63 cells. Before the cell seeding, the scaffolds were soaked in cell culture media for 24 h. Then, each scaffold was seeded by carefully dropping 10 μL of cell suspension ( $30.0 \times 10^3$  cells) onto their upper surface, allowing cell attachment for 30 min at 37 °C before adding complete cell culture media. The cells were grown for three days onto the scaffold to obtain complete colonization of the material, namely the 3D OS model (0 h); then, the medium was changed and substituted with the GO@PEG-Pt-DOX – conditioned media. Pt-DOX was used as control, and the no-seeded scaffold was used as blank. The in vitro 3D OS models were cultured in the presence of the compounds for 72 h. The conditions of the 3D OS model grown in standard cell media were used as negative control (cells only). All cell handling procedures were performed under a laminar flow hood in sterility conditions.

**Cell Viability Assay:** Cell viability was assessed after 72 h of culture with the compounds in both the 2D cell cultures and the 3D OS models by performing the MTT assay, following the manufacturer's instructions. Briefly, the 2,5-diphenyltetrazolium bromide (MTT) reagent (Sigma Aldrich) was dissolved in Phosphate Saline Buffer 1X (PBS 1X, Gibco) at the concentration of 5 mg mL<sup>−1</sup>. Then, the MTT solution was added to each well in a 1:10 volume ratio and incubated for two hours at 37 °C. The media was removed, and, for the 2D cell cultures, the formazan crystals derived from MTT conversion by metabolically active cells were dissolved in 200 μL of Dimethyl Sulfoxide (DMSO, Sigma Aldrich) for 15 min incubation at RT in stirring conditions. For the 3D OS models, the scaffolds were transferred to a tube with 500 μL of DMSO and mechanically broken using pestles to release the formazan crystals produced by the cells. Then, the samples were centrifuged, and 200 μL of each supernatant in duplicate was analyzed. In both studies, the absorbance was read at λ<sub>max</sub> 570 nm using the Multiskan FC Microplate Photometer (ThermoFisher Scientific), and it is proportionally related to the number of metabolically active cells ( $n = 3$ ).

**Cell Morphology and Scaffold Colonization Evaluation:** The 3D OS models were deeply characterized in terms of the scaffold's cell morphology and colonization level. For both types of analysis, the 3D OS models were cultured for 72 h in the presence of GO@PEG-Pt-DOX, using the models with Pt-DOX and cells only as control groups. For the cell colonization analysis, the 3D OS model at 0 h, represented by the 3 days colonized scaffold before the addition of compounds (see at the "3D cell culture model" paragraph for more details), was used as further control.

For both analyses, the 3D OS model at 0 h and 72 h was removed from the cell media, washed with PBS 1X and fixed with 4% paraformaldehyde (PFA) (Sigma Aldrich) for 15 min at RT. Then, the cells were washed with PBS 1X twice and 0.1% v/v Triton X-100 (Sigma Aldrich) was added to permeabilize the cells. To assess the cells' well-being and cytoskeleton integrity, the 3D OS models were incubated with ActinRed 555 ReadyProbes reagent (Invitrogen) for 30 min and the cell nuclei were counterstained with 4',6-diamidino-2-phenylindole dihydrochloride (DAPI, 600 nm) (Invitrogen) reagent for 10 min. The 3D OS models were then imaged by DAPI and TRITC filters using an Inverted Ti-E Fluorescent Microscope (Nikon). For the cell migration analysis, the 3D OS models were sectioned, and six random measurements were taken for each group using NIS-Elements software (Nikon) to determine the distance (in μm) migrated by the cells from the seeding surface to the inner region of the scaffold (Figure S4, Supporting Information). The data were normalized with respect to the 3D OS model at 0 h, to assess their potential inhibitory activity on cell migration (i.e., scaffold colonization) at 72 h ( $n = 2$ ).

**Statistical Analysis:** All the results are reported in graphs as the mean ± standard deviation (SD). Cell viability results were analyzed by GraphPad Prism Software (Version 8.0) by applying a two-way ANOVA statistical test followed by Dunnett's and Tukey's multiple comparisons test. Cell colonization results were analyzed by using a one-way ANOVA statistical test followed by Tukey's multiple comparisons

test. The statistical significance obtained is represented in graphs as follows: \* $p$ -value  $\leq 0.05$ , \*\* $p$ -value  $\leq 0.01$ , \*\*\* $p$ -value  $\leq 0.001$ , and \*\*\*\* $p$ -value  $\leq 0.0001$ .

## Supporting Information

Supporting Information is available from the Wiley Online Library or from the author.

## Acknowledgements

This work has been funded by the European Project Horizon 2020 NANO4TARMED (H2020-WIDESPREAD-2020-5; GA number 952063). The work was supported by the MEYS CR (Large RI Project LM2018129 Czech-Biolmaging) and by the project National Institute for Cancer Research (Programme EXCELES, ID Project No. LX22NPO5102) - Funded by the European Union-Next Generation EU. The work was supported by ERDF/ESF project TECHSCALE (No. CZ.02.01.01/00/22\_008/0004587). [Correction added on 6 July 2024, after first online publication: The funding information has been updated in acknowledgements section.]

## Conflict of Interest

The authors declare no conflict of interest.

## Author Contributions

M.M., S.P., D.M., and V.R. Conceptualization; L.Z., E.M., A.R., M.G.C., E.C., G.B., and P.B. Investigation; E.G., L.Z., A.R., G.B., A.R., and P.B. Analyzed the data; L.Z., A.R., G.B., D.M., and S.P. Writing- original draft preparation; D.M., S.P., and V.R. Writing-review and editing; S.P., D.M., and V.R. Funding acquisition. All authors have read and agreed to the published version of the manuscript.

## Data Availability Statement

The data that support the findings of this study are available on request from the corresponding author. The data are not publicly available due to privacy or ethical restrictions.

## Keywords

anticancer treatment, cisplatin, doxorubicin, graphene oxide, nanomedicine

Received: March 8, 2024

Revised: May 6, 2024

Published online:

- [1] M. I. Khan, M. I. Hossain, M. K. Hossain, M. H. K. Rubel, K. M. Hossain, A. M. U. B. Mahfuz, M. I. Anik, *ACS Appl. Bio Mater.* **2022**, *5*, 971.  
[2] A. K. Geim, K. S. Novoselov, *Nat. Mater.* **2007**, *6*, 183.

- [3] O. Akhavan, E. Ghaderi, S. Aghayee, Y. Fereydooni, A. Talebi, *J. Mater. Chem.* **2012**, *22*, 13773.  
[4] E. Khakpour, S. Salehi, S. M. Naghib, S. Ghorbanzadeh, W. Zhang, *Front. Bioeng. Biotechnol.* **2023**, *11*, 1129768.  
[5] A. M. Itoo, S. L. Vemula, M. T. Gupta, M. V. Giram, S. A. Kumar, B. Ghosh, S. Biswas, *J. Controlled Release* **2022**, *350*, 26.  
[6] E. Aliyev, V. Filiz, M. M. Khan, Y. J. Lee, C. Abetz, V. Abetz, *Nanomaterials* **2019**, *9*, 1180.  
[7] A. A. D'souza, R. Shegokar, *Expert Opin. Drug Delivery* **2016**, *13*, 1257.  
[8] M. Orecchioni, R. Cabizza, A. Bianco, L. G. Delogu, *Theranostics* **2015**, *5*, 710.  
[9] X. Zhao, J. Si, D. Huang, K. Li, Y. Xin, M. Sui, *J. Controlled Release* **2020**, *323*, 565.  
[10] G. Agrawal, R. Agrawal, *ACS Appl. Nano Mater.* **2019**, *2*, 1738.  
[11] V. Sauraj, B. Kumar, R. Priyadarshi, F. Deeba, A. Kulshreshtha, A. Kumar, G. Agrawal, P. Gopinath, Y. S. Negi, *Mater. Sci. Eng., C* **2020**, *10*, 110356.  
[12] S. Li, T. Zhang, W. Xu, J. Ding, F. Yin, J. Xu, W. Sun, H. Wang, M. Sun, Z. Cai, Y. Hua, *Theranostics* **2018**, *8*, 1361.  
[13] X. Yang, C. Hu, F. Tong, R. Liu, Y. Zhou, L. Qin, L. Ouyang, H. Gao, *Adv. Funct. Mater.* **2019**, *29*, 1901896.  
[14] Y. Liu, X. Zhang, M. Zhou, X. Nan, X. Chen, X. Zhang, *ACS Appl. Mater. Interfaces* **2017**, *9*, 43498.  
[15] E. Giusto, L. Žárská, D. F. Beirne, A. Rossi, G. Bassi, A. Ruffini, M. Montesi, D. Montagner, V. Ranc, S. Panseri, *Nanomaterials* **2022**, *12*, 2372.  
[16] X. Ma, H. Tao, K. Yang, L. Feng, L. Cheng, X. Shi, Y. Li, L. Guo, Z. Liu, *Nano Res.* **2012**, *5*, 199.  
[17] J. Chen, H. Liu, C. Zhao, G. Qin, G. Xi, T. Li, X. Wang, T. Chen, *Biomaterials* **2014**, *35*, 4986.  
[18] I. Corre, F. Verrecchia, V. Crenn, F. Redini, V. Trichet, *Cells* **2020**, *9*, 976.  
[19] J. Ritter, S. S. Bielack, *Ann. Oncol.* **2010**, *21*, vii320.  
[20] R. Rathore, B. A. Van Tine, *J. Clin. Med.* **2021**, *10*, 1182.  
[21] M. Weller, W. Wick, K. Aldape, M. Brada, M. Berger, S. M. Pfister, R. Nishikawa, M. Rosenthal, P. Y. Wen, G. Roger Stupp, *Nat. Rev. Dis. Primers* **2015**, *1*, 15017.  
[22] R. Edmondson, J. J. Broglie, A. F. Adcock, L. Yang, *Assay Drug Dev. Technol.* **2014**, *12*, 207.  
[23] P. Horvath, N. Aulner, M. Bickle, A. M. Davies, E. Del Nery, D. Ebner, M. C. Montoya, P. Östling, V. Pietiäinen, L. S. Price, S. L. Shorte, G. Turcatti, C. von Schantz, N. O. Carraghe, *Nat. Rev. Drug Discovery* **2016**, *15*, 751.  
[24] G. S. Krishnakumar, N. Gostynska, M. Dapporto, E. Campodoni, M. Montesi, S. Panseri, A. Tampieri, E. Kon, M. Marcacci, S. Sprio, M. Sandri, *Int. J. Biol. Macromol.* **2018**, *106*, 739.  
[25] S. Choi, A. M. Bhagwat, R. Al Mismar, N. Goswami, H. B. Hamidane, L. Sun, J. Graumann, *Sci. Rep.* **2018**, *8*, 5858.  
[26] R. G. Kenny, C. J. Marmion, *Chem. Rev.* **2019**, *119*, 1058.  
[27] S. Stankovich, D. A. Dikin, R. D. Piner, K. A. Kohlhaas, A. Kleinhammes, Y. Jia, Y. Wu, S. T. Nguyen, R. S. Ruoff, *Carbon* **2007**, *45*, 1558.  
[28] H. C. Schniepp, J. L. Li, M. J. McAllister, H. Sai, M. Herrera-Alonso, D. H. Adamson, R. K. Prud'Homme, R. Car, D. A. Saviile, I. A. Aksay, *J. Phys. Chem. B* **2006**, *110*, 8535.  
[29] I. Jung, M. Pelton, R. Piner, D. A. Dikin, S. Stankovich, S. Watcharotone, A. M. Hausner, R. S. Ruoff, *Nano Lett.* **2007**, *7*, 3569.